Indian Journal of Pure & Applied Physics
Vol. 62, February 2024, pp. 164-175
DOI: 10.56042/ijpap.v62i2.7753

Antibacterial and Hydrophobic Graphite-siloxane Composite Coating towards Microbial Corrosion Resistant Application of Steel: Experimental and Theoretical Insight

Swarnima Singh[a], Dibya Singh Pradhan[a], Pratap Mane[b], Upasana Mohapatra[c], Sony Pandey[c], Bimal Prasad Singh[a], Brahmananda Chakraborty[b,d*] & Sriparna Chatterjee[a*]

[a]Materials Chemistry Department, CSIR-Institute of Minerals and Materials Technology, Bhubaneshwar 751 013, India
[b]Seismology Division, Bhabha Atomic Research Centre, Trombay, Mumbai 400 085, India
[c]Environment & Sustainability Department, CSIR-Institute of Minerals and Materials Technology, Bhubaneshwar 751 013, India
[d]High Pressure and Synchrotron Radiation Physics Division, Bhabha Atomic Research Centre, Trombay, Mumbai 400 085, India

Received 3 January 2024; accepted 23 January 2024

The fabrication of hydrophobic graphite-siloxane composite coating on low carbon steel (LCS) substrate using electrophoretic deposition is reported. At a critical concentration (~ 20 wt. %) of methyl hydrogen polysiloxane (trade name KF-99), it achieved the highest hydrophobicity of the composite coating (Contact angle ~122º). The corrosion resistance of the hydrophobic composite coating is examined in 3.5 wt—% NaCl solution. The potentiodynamic curves demonstrate that the corrosion rate is drastically reduced to 79.3 % for graphite-siloxane composite coating (cured at 400 ºC) than bare LCS substrate. Both grain refinement due to heat treatment and increment in water contact angle significantly contribute to increased corrosion resistance.Additionally, it is observed that graphite–siloxane composite coating shows good antibacterial properties, which may enable the coating to combat microbial corrosion of metals. To support the experimental findings, we have studied the interactions of water molecules on low-carbon steel and the hybrid structure of LCS/graphite and tri-layer LCS/ graphite/siloxane using sophisticated Density Functional Theory simulations. The adsorption energy data reflect that water strongly interacts with LCS, but interactions become weak with LCS/graphite and hydrophobic for LCS/graphite/siloxane, supporting the experimental data. There is a reduced interaction between the O 2p orbital of H_2O with LCS with the addition of graphite, which further shows a drastic reduction with siloxane. The low H2O adsorption energy and reduced charge transfer from H_2O to LCS in the presence of graphite-siloxane composites can confirm this.

Keywords: Graphite; Siloxane; Coating; Hydrophobicity; Corrosion; Antibacterial

1 Introduction

Low carbon steel (LCS) is extensively used in the construction industry, marine application, nuclear power plants, fossil fuel plants, transportation, chemical processing, metal-processing equipment, mining, petroleum production, and refining due to its high workability, excellent weldability, ultimate tensile strength (440 MPa), and many other[1-4] unique properties. However, all these applications require long-term service in the extreme environment, and wear and tear like high-temperature oxidation, aqueous corrosion, and abrasion[3,5-6] play a significant role in long-term service. At this point, the need for efficient, cheaper, and long-lasting anti-corrosion coating arises for the comprehensive and long-term application of LCS that can survive in an extreme environment. Several researchers have worked on the corrosion behavior of Ni-P, Ni-Cr-P, Ni-Cr, and graphene coatings on low carbon steel using electrochemical routes[7-10]. However, nickel coatings are not resistant to nitric acid and environments containing chloride. In addition, the deposition of chromium in coatings involves environmental hazards because of carcinogenic hexavalent chromium (Cr^{6+}) ions[7]. Although graphene-based coatings render efficient anti-corrosion properties, however, large-scale production of graphene is not economically viable. One plausible solution could be the use of graphite as a coating material because of its intrinsic layered structure, reasonable specific surface area (90 m^2/g)[11], compression strength (~ 200 MPa), good electrical conductivity and thermal conductivity (~ 25-470 W/mK)[12], biocompatibility, lubrication property, easy availability, *etc*.[7-9].

*Corresponding author:
(E-mail: sriparna@immt.res.in; brahma@barc.gov.in)

However, there are a handful of reports on the large-scale fabrication of graphite coating as researchers have primarily relied on sophisticated techniques like screen-printing[14], a combination of plasma electrolytic oxidation (PEO), and electrophoretic deposition (EPD)[13], *etc*. Arun *et al*. reported that nano-sized graphite particles efficiency is more than micro-sized particles[13]. Here, we have developed graphite-siloxane composite coating on LCS using the electrophoretic deposition (EPD) process. The EPD process is a modest and versatile method to fabricate coatings on a wide range of substrates[15] with advantages such as scale-up, easy control over stoichiometry, better uniformity, *etc*.[15-16]. The graphite coating is prepared on LCS by a simple one-step EPD followed by post-treatment with methyl hydrogen polysiloxane and is further heat-treated at two different temperatures (*i.e*., 400 and 600 ºC). The siloxanes are proven to facilitate the anticorrosion behavior of different kinds of coatings, including graphene oxide, ceramic, *etc*.[17-18].

In this work, the effect of siloxane on the development of composite coating is studied through different physicochemical characteristics of coatings and is correlated with their anticorrosion behavior. To the best of our knowledge, this is the first report on the graphite-siloxane composite coating on LCS for high-temperature applications. Following the work of Shaobin *et al*.[19] antimicrobial properties of the composite coatings are also studied as microbial corrosion is another crucial aspect that needs to be addressed for the longevity and durability of oil pipelines. Therefore, this study is vital to render an amicable solution to different types of corrosion-related issues on steel surfaces.

To analyse the hydrophobic nature of graphite - siloxane composite with LCS we have done the first principle calculations. The electronic properties, orbital interactions, charge transfer and isosurface charge distribution have been presented for LCS combined with graphite and graphite - siloxane composites.

2 Experimental details

2.1 Electrophoretic deposition of graphite–siloxane composite coating on LCS substrate

LCS (AISI 1018) plate (4 cm ×1.5 cm × 0.3 cm) is used as a substrate for the EPD process. Before EPD, the LCS substrates are polished with emery paper (120 grit size) and ultrasonically cleaned with acetone for 30 minutes. Then 1.0 gram of graphite nanopowder (95 %, CDH chemicals) is dispersed in 50 ml of acetone (Finar) and ultrasonicated (Model: CVX-130PB, power output 130 V and frequency 20 kHz, Sonics & Materials Inc, Newtown CT, USA) for 2 hours. All depositions are carried out at a potential of 10V using a source meter at constant current mode (Model: 2410, Keithley Instruments, Inc, USA), and deposition time is fixed at 3 minutes. The green coating is dried at room temperature for 24 hours and then dipped in a mixture of 20 % KF-99 and 80 % ethanol and allowed to dry for 24 hours and then heat-treated at 140, 400, 600 and 750 ºC for 2 hours. Henceforth, the samples will be identified as G-140, G-400, G-600 and G-750 ºC respectively**.**

2.2 Characterizations

The cross-sectional and surface morphologies of all the samples are studied using field emission scanning electron microscopy (FE-SEM) (JSM – 6010LA, JEOL, Japan).

The phase purity is determined using an X-ray diffraction study (Rigaku, TTRAX III, Japan). The crystallite size is calculated using Scherrer Eq. 1 and micro-strain is calculated by using Eq. 2

$$D = \frac{0.9\,\lambda}{\beta\, Cos\theta} \quad \ldots (1)$$

$$\varepsilon = \frac{\beta}{4tan\,\theta} \quad \ldots (2)$$

Where D is crystallite size, λ is wave number of X-ray radiation, β is full-width half maxima, θ is Bragg angle and Ɛ is micro-strain[4,20].

Raman spectra are obtained in the scan range of 100 - 2000 cm^{-1} using a Renishaw Imaging Microscope WiRE (Model: Invia Reflex-H33197, Incoterm, UK) using a 532 nm wavelength Ar laser.

The pristine graphite powder and composite coatings are also characterized using Fourier transform infrared (FTIR) spectroscopy (Model: Varian 800, Japan) to ascertain the interaction between graphite and siloxane with the substrate.

The contact angles (CA) of all samples are measured at room temperature and at a relative humidity of 51% using 2 μL droplets of Milli-Q water using a goniometer (OCA-35, Data Physics). The CA measurements are done at different positions of coating to check uniformity.

2.3 Antibacterial Activity Test

The antibacterial performance of the bare LCS (as control), G-400 and G-600 ºC coatings are tested against gram-negative bacteria *i.e*., Escherichia coli. The test organism is inoculated in 25 mL of nutrient

agar (Hi-Media) and incubated at 37 ºC for up to 24 hours to obtain a broth culture. The graphite–siloxane composite coated and uncoated substrate is then spot inoculated at well-marked places with 5µL of the E.coli broth culture at a cell concentration of 10^8 cells/mL and incubated at 37 ºC in a moist chamber to avoid the drying of the culture droplet. After incubation, the cells were harvested from the samples and collected in Nutrient Broth solution and 0.1 mL of it was spread on Nutrient Agar plates and incubated again at 37 ºC to check the cell viability and growth on the coated and uncoated surfaces.

2.4 Electrochemical Corrosion Test

The electrochemical characterizations of the samples are carried out in 3.5 wt. % NaCl solution using a source meter (Chi 660D, Austin, U.S.A). The coated, as well as bare substrate, are served as a working electrode with an exposure area of (1 × 1 cm^2), whereas Ag/AgCl and platinum wire are used as a reference and as a counter electrode respectively. Before the electrochemical test, all the samples are cleaned using acetone and distilled water. The OCP measurement is performed for two hours for all the samples to attain stability. An anodic polarization test is carried out by scanning the samples from cathodic region -1 V to anodic region 1 V with respect to OCP. All the electrochemical tests are repeated three times to ascertain reproducibility. The corrosion rates of bare and coated LCS are estimated using Equation 3 following the American Society for Testing and Materials (ASTM) standard G102[21].

$$\text{Corrosion Rate} = \frac{\text{K}\, i_{corr}}{\rho\, \text{A}} \times \text{EW} \qquad \ldots (3)$$

Where K is the Corrosion Rate constant (1.288 × 10^5 mili per A cm year), EW is the equivalent weight of the LCS (28.25 g), ρ is the density of LCS (7.87 g/cm^3), and A is the surface area of the samples (1×1 cm^2).

2.5 Computational details

With the aid of Density Functional Theory as implemented in VASP code[22-25] the geometrical optimizations and electronic state calculations were performed. The Perdew-Burke-Ernzerhof (PBE) based projector augmented wave (PAW) scheme was used for this study. The generalized gradient approximation (GGA) with PBE pseudo-potentials were applied as the exchange-correlation functional[26]. The cut off energy was taken as 520 eV and the Brillion zone sampling were done with a Monkhorst pack[27] mesh of 5x5x1 and 7x7x1 for atomic optimizations and electronic states analysis respectively. The atomic optimizations were carried out till the forces and energy convergence criteria reached to 0.01 eV/Å and 10^{-6} eV respectively. All the calculations were done within the spin-polarized Density Functional Theory framework. To avoid the interaction and repetition of layers a vacuum of 20 Å was introduced along the z direction which is perpendicular to the atomic planes.

3 Results and Discussion

The X-ray diffraction patterns of bare LCS, pristine graphite powder, and G-400 and G-600 ºC are represented in Fig. 1(a) (a-d). The bare LCS sample shows diffraction lines at 2θ = 44.7°, 65.0°, and 82.3° that correspond to (110), (200), and (211) planes of body-centered cubic (BCC) structure of Fe (JCPDS card number: 087-0721). Graphite powder, G - 400 ºC, and G - 600 ºC coatings show a prominent peak at 25= 26.5º, which indicates the complete coverage of LCS substrate by the graphite. The crystallite sizes are calculated using the Scherrer formula (Eq. 1), and the micro-strain is calculated using Equation 2. The crystallite size of graphite powder is 4.92 nm. For G-400 ºC, the crystallite size is 2.13 nm, and for G-600 ºC is 2.03 nm. A steady decrease in crystallite size is observed as sintering temperature, or annealing temperature is increased. Such decrement in crystallite size may occur due to the pinning effect of graphite particles present in the coating[28].

Crystallite size may also decrease because of impeded dislocation movement of the graphite particles. Graphite particles may restrain grain growth, and eventually, high-stress accumulation may be encouraged. Because of high-stress accumulation, a high lattice micro-strain is generated, which is reflected for G-400 and G-600 ºC. The exact values of crystallite size and micro-strain are presented in Table 1. An increase in the lattice micro-strain values is attributed to lattice defects such as vacancies, substitutions, and interstitial atomic impurities. These defects could be occurred due to the diffusion of elements during the heat-treatment process.

Figure 1(b) elucidates the Raman spectra of the pristine graphite powder, G-400 and G-600 ºC coatings. The powder and coatings exhibit a D band at 1350 cm^{-1} and a G band at 1590 cm^{-1}, respectively. The presence of a G band and D band confirms the graphitic structure and defect density in the powder

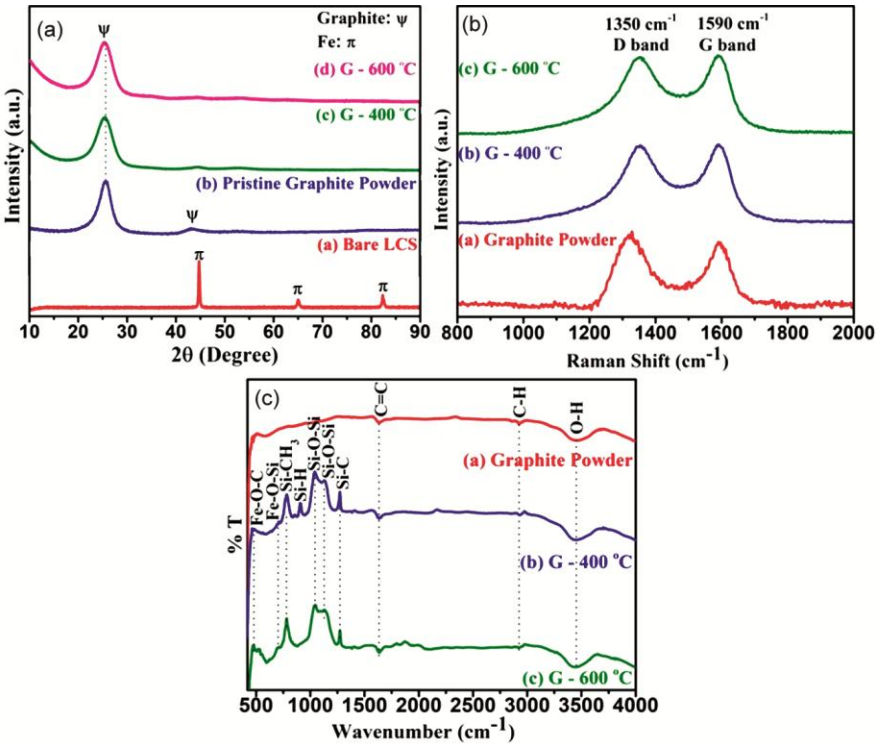

Fig. 1 — Shows the (a) XRD pattern of bare LCS, (b) Raman spectra and (c) FT-IR of pristine graphite powder and electrophoretic deposited graphite coatings heat-treated at 400 ºC and 600 ºC.

Table 1 — Shows crystallite size, lattice strain and I_D/I_G ratio of bare LCS, pristine graphite powder, G – 400 ºC and G – 600 ºC coatings

S No.	Sample	Crystallite Size (nm)	Lattice Strain	I_D/I_G Ratio
1.	Bare LCS	33.71	0.0055	-
2.	Graphite Powder	4.92	0.0704	1.34
3.	G - 400 ºC	2.13	0.1525	1.72
4.	G - 600 ºC	2.03	0.1708	1.80

and coatings. Moreover, the defect formations in coatings are examined by calculating the I_D/I_G ratio, which measures the intensity of the defect to graphitization. The I_D/I_G ratio of the powder and graphite coatings values has been tabulated in Table 1. The I_D/I_G ratio of as-received graphite powder is 1.34, which is enhanced to 1.72 for G-400 ºC sample, further it is increased to 1.80 for G-600 ºC coating. This increment in I_D/I_G ratio may be attributed to the loss of a hydrogen atom from the sp^3 domain, resulting in the graphitization of C-C sp^3 to C-C sp^2 carbon[29].

The formation of intermetallic compounds is established through FT-IR analysis. Fig. 1(c) displays the FT-IR spectra of pristine graphite powder, G-400 and G-600 ºC coatings. The OH stretching is observed in the broad band at 3453 cm^{-1}, which signifies the hydroxyl or absorbed H_2O present in pristine graphite powder and heat-treated coatings. The C-H bond stretching vibrations of the groups -CH_2 (2925 cm^{-1}) are also observed in graphite powder and coatings. Further, carbon bond C=C is also noticed at 1632 cm^{-1} which could be due to unoxidized graphitic carbon present in graphite powder and coatings. The emergence of new peaks is identified in G-400 and G - 600 ºC coatings at 1272 cm^{-1} corresponding to Si-C, 1126 cm^{-1}, and 1036 cm^{-1} to Si-O-Si, 779 cm^{-1} to Si-CH_3, 702 cm^{-1} to Fe-O-Si, 473 cm^{-1} to Fe-O-C. These peaks are due to KF-99 and its interaction with graphite during the curing process. Hence, Si-O-Si bonding could be attributed to the cross-linked structure formed while curing coatings. It helps in restricting water molecules and corrosive ions from penetrating the coating. The emergence of a new peak is seen in G-400 ºC coating at 904 cm^{-1} signifies a Si-H bond. The formation of Fe-O-Si and Fe-O-C bonding helps to improve coating adhesion.

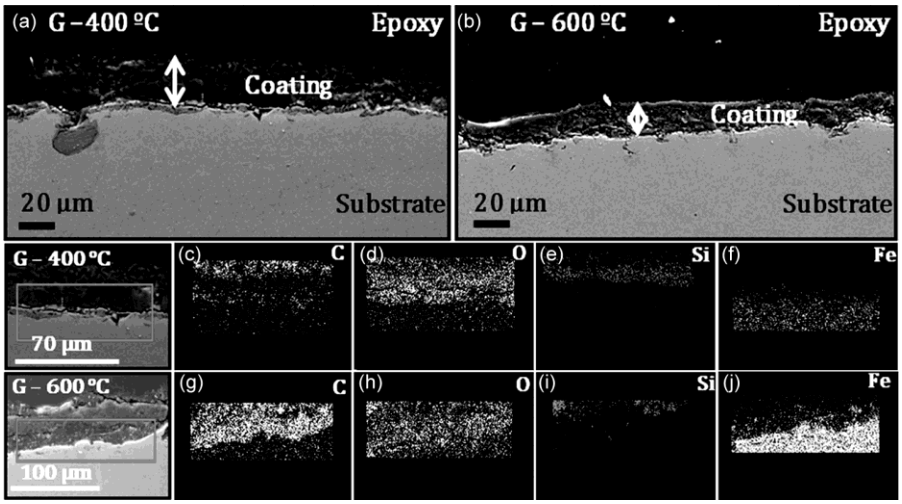

Fig. 2 — (a-b) Cross-sectional images of electrophoretically deposited graphite coatings heat-treated at G - 400 ºC and G – 600 ºC and (c-j) shows the X-ray mapping of C, O, Si, and Fe elements.

Figure 2(a-b) displays the cross-sectional FE-SEM images of graphite-siloxane composite coatings heat-treated at 400 and 600 ºC. An increase in heat treatment temperature from 400 to 600 ºC shows a decrease in coating thickness from 23 ± 1 µm to 14 ± 1 µm. The formation and growth of intermetallic compounds in the bonding interface of iron and carbon with increasing temperature may lead to a decrease in coating thickness[30-31]. X-ray mapping is carried out on cross-sections of G - 400 and 600 ºC to confirm the diffusion of elements. Fig. 2(c-j) shows the elemental mapping of Carbon (C), Oxygen (O), Silicon (Si), and Iron (Fe).

From the images, the diffusion of Si into substrate and Fe into coating is evident. With the increase in annealing temperature, the diffusion of iron into the coating is more. Interestingly, short-range movements of atoms are present in G-400 ºC sample, which is called structural changes within the grain boundaries. However, at a higher temperature, additional vacancies may be generated and that may enhance the diffusion of elements and in some cases, the formation of intermetallic compounds is also observed[32].

Figure 3(a-f) shows the surface morphology of graphite powder and graphite-siloxane composite coatings. The pristine graphite powder shows a flakes kind of morphology, while G-400 and G - 600 ºC coatings show a uniform and smooth texture (Fig. 3(a-c)). A detailed look at G - 600 ºC shows cracks (Fig. 3(d)). These cracks may generate due to the stress caused by volume change that occurred during the heat-treatment process. Tsui *et al*. have also observed

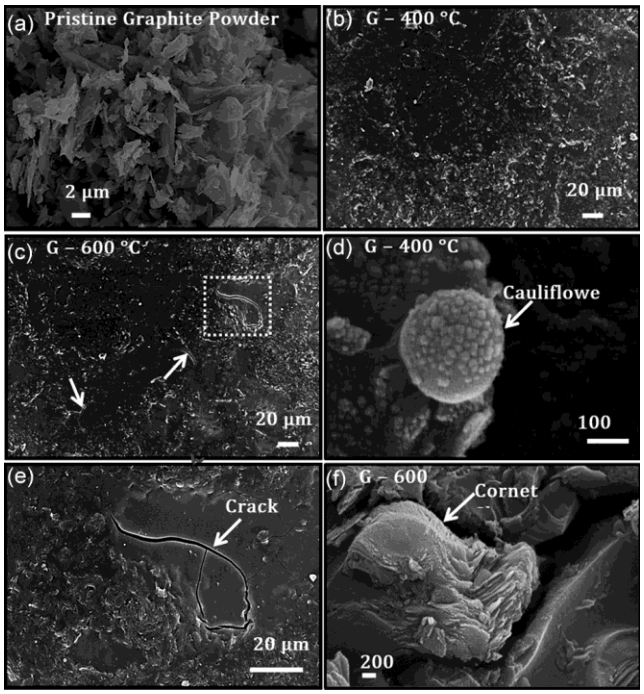

Fig. 3 — Surface morphology of (a) Pristine graphite powder (b) Electrophoretic deposited graphite coatings heat-treated at (b) 400 ºC (c) 600 ºC (d) high magnified image from G - 600 ºC coating showing micro-crack and (e-f) highly magnified view from (b-c) showing cornet and cauliflower microstructure.

cracking in thermally treated hydroxyapatite coating at 700 ºC and reported similar findings[33].

However, cracks in G - 600 ºC coatings could be responsible for the penetration of chloride ions from the electrolyte into the surface, resulting in the formation of large pits and degrading the material. The corrosion behavior of bare LCS, G-400 and G - 600 ºC coatings is discussed later. Fig. 3(e-f) shows

the high magnification images from G-400 and G-600 ºC coatings revealed a fascinating morphology similar to cornet and cauliflower shape, respectively. Further, tiny irregular-shaped nanograins are also seen over cornet and cauliflower shapes (Fig. 3(e-f)).

Figure 4(a) displays the plot of time versus open circuit potential (OCP) for bare LCS, G-400 and G-600 ºC coatings in 3.5 wt. % NaCl solution. It is observed that the OCP value shifts towards a more positive side for the composite coatings than bare LCS, which indicates the corrosion resistance behavior of coated substrate. The bare LCS has the lowest potential value of - 0.51 V, whereas G-400 and G-600 ºC shows potential values of - 0.42 V and - 0.44 V respectively. This increment in OCP may be related to the presence of the stable film on coated substrates.

The polarization curves of all samples are exploited to evaluate corrosion potential (E_{corr}), corrosion current density (i_{corr}), and corrosion rates (CR). The individual values of E_{corr}, i_{corr}, and CR has been tabulated in Table 2. Fig. 4(b) shows that E_{corr} moved towards the more positive potential for G-400 and G-600 ºC coatings compared to bare LCS. A reduction in i_{corr} up to 79.32 % and 46.38 % are observed for G-400 and G-600 ºC as compared to bare LCS. Interestingly, i_{corr} value of the G-600 ºC sample is more than G-400 ºC. This may happen because of the presence of micro-cracks in the G-600 ºC sample (Fig. 3(d)). These micro-cracks may provide an easy path for chloride ions to penetrate through the substrate, leading to reduced corrosion resistance. It is known that i_{corr} is directly proportional to the corrosion rate; therefore, the corrosion rate of G-400 ºC (8.74×10^{-3} mpy) is lower than G-600 ºC (22.69×10^{-3} mpy) sample. Furthermore, corrosion inhibition efficiency (η) of G - 400 and G-600 ºC is calculated using Eq. 4[21]. G-400 ºC shows the highest inhibition efficiency, up to 79.32 %, among all three samples.

$$\eta = \frac{I_{corr\ (Bare\ )} - I_{corr\ (coated\ )}}{I_{corr\ (Bare\ )}} \times 100 \quad \ldots (4)$$

where I is the polarized current density superior corrosion resistance behavior of G-400 ºC sample may be attributed to the following reasons: (i) reduction in grain refinement after heat treatment (ii) formation of SiC particle which may help in lowering the metallic area required for corrosion (iii) due to hydrophobicity the coating surface hinder the penetration of chloride ions to the metal surface (iv) strong interfacial bonding due to formation of bonds like Fe-O-Si, Fe-O-C, and Si-O-Si. The effect of

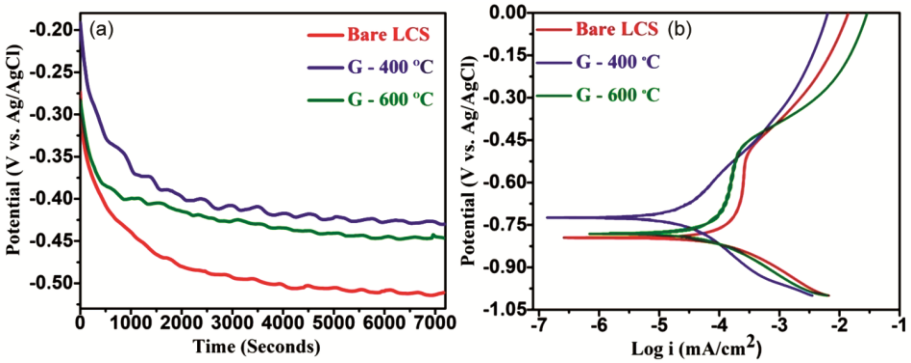

Fig. 4 — shows the (a) open circuit potential and (b) polarization curve of bare LCS, Electrophoretically deposited graphite-siloxane composite coating heat-treated at 400 ºC and 600 ºC in 3.5 wt. % NaCl solutions.

Table 2 — Showing i_{corr}, E_{corr}, corrosion rate, and inhibition efficiency value of bare LCS and Electrophoretic deposited graphite-siloxane composite coating heat-treated at 400 ºC and 600 ºC in 3.5 wt. % NaCl solutions.

S No.	Nomenclature	i_{corr} ($\mu A/cm^2$) × 10^{-2}	E_{corr} (V vs. Ag/AgCl)	Corrosion Rate(mpy)× 10^{-3}	Inhibition Efficiency (%)
1.	Bare LCS	9.14	-0.79	42.26	-
2.	G - 400 ºC	1.89	-0.72	8.74	79.32
3.	G - 600 ºC	4.90	-0.78	22.69	46.38

electrochemical polarization on coated samples is studied using FESEM. Fig. 5(a-c) displays the surface morphology of bare LCS, G-400 and G-600 ºC after the polarization test carried out in 3.5 wt. % NaCl solutions. It is evident from the Fig. 5, that the presence of pits is less in coated samples as compared to bare ones because graphite and SiC particles restrict the penetration of Cl^- ions to the substrate surface. The presence of elemental chlorine after the polarization test is confirmed by EDX mapping. The bare LCS has a higher amount of chlorine on the surface, which implies its highest susceptibility to corrosion. G-600 ºC coating has relatively lesser chlorine content, and it is drastically reduced for G-400 ºC sample. This confirms the formation of a uniform protective layer that acted as a blanket for the substrate of the G-400 ºC sample.

The wettability of composite coatings is a crucial issue as it controls the anticorrosion behavior of the substrate. Bare LCS is hydrophilic with a water contact angle of 78.6º (Fig. 6(a)) whereas graphite - siloxane coated LCS substrates (*i.e.*, G-400 and G-600 ºC) show hydrophobic behavior with a water contact angle of 122º and 116º (Fig. 6(b-c)) respectively. Along with the intrinsic hydrophobic nature of graphite, the surface microstructure of the

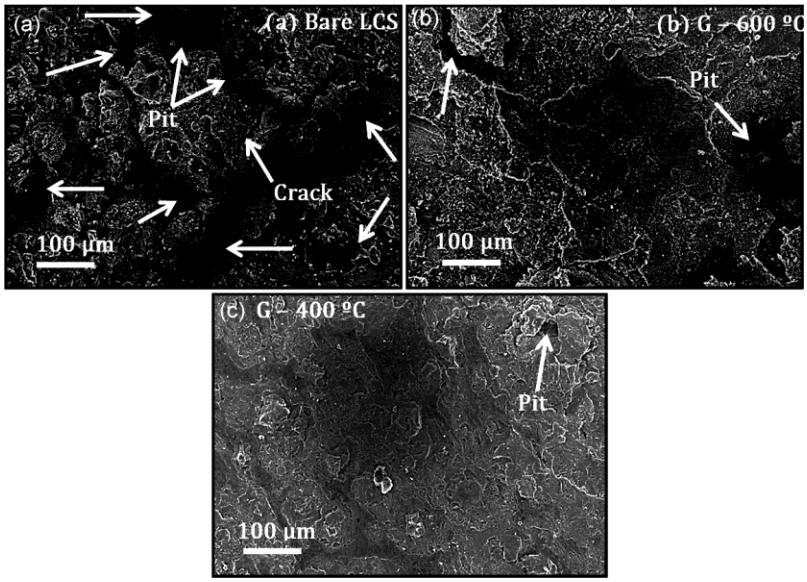

Fig. 5 — Surface morphology shows pits after anodic polarization test in (a) Bare LCS and (b-c) Electrophoretic deposited graphite-siloxane composite coatings heat-treated at 400 ºC and 600 ºC, after anodic polarization test in 3.5 wt. % NaCl solution.

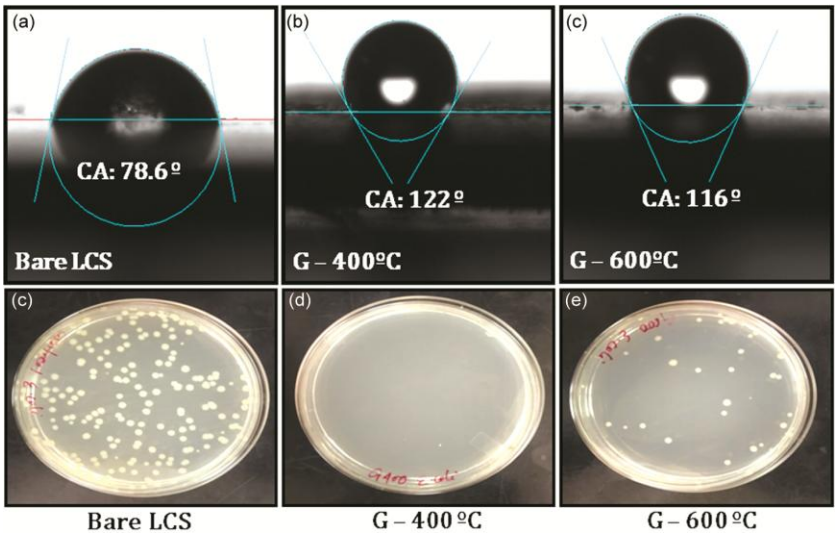

Fig. 6 — (a-c) Contact Angle and (d-f) Viable cells of E.coli grown on NA plates from Bare LCS and Electrophoretically deposited graphite-siloxane coatings heat-treated at 400 ºC and 600 ºC.

composite coatings also contributes to hydrophobicity. The FE-SEM image of both G-400 and G-600 ºC showed the presence of hierarchical structures (Fig. 3(e-f)) in the form of cornet and cauliflower shapes. Such unique microstructures (cornet and cauliflower structure) render water repellence by trapping air in the gaps between adjacent micro/nanostructures[34]. The slight decrement in contact angle for G-600 ºC composite coatings may be attributed to cracks in the surface. Pinning of water droplets may occur through the micro-cracks generated during heat treatment at 600 ºC. Other than the presence of micro-cracks, M-O-Si moiety also contributes to lowering the contact angle. The organic part (methyl groups) of KF-99 is broken during the annealing of the green coating, leaving behind an M-O-Si moiety. This M-O-Si attracts water molecules and tends to make the coated surface hydrophilic. Annealing at a higher temperature (*i.e*., 600 ºC) will give rise to a more significant fraction of M-O-Si moiety, and as a result, the water contact angle is decreased compared to the coating, which is annealed at 400 ºC. These hydrophobic coatings are expected to act as an inert physical barrier to the corrosive NaCl electrolyte.

Shoabin *et al*. reported the cytotoxicity effect of graphene oxide nanoparticles on bacteria[19]. This study intrigued us to estimate the antibacterial effect of the graphite-siloxane composite coatings. Fig. 6(d-f) represents the effect of bare LCS, G-400 and G-600 ºC coatings when subjected to a cultured E. Coli environment. Fig. 6(d) shows the highest number of colonies (*i.e.*, 182 colonies) as compared to the other two sets (Fig. 6(e-f)). This implies that bare LCS substrate does not show any antibacterial property, whereas G-400 ºC coating is best (1 colony). G-600 ºC coating shows moderate antibacterial properties (30 colonies). The antibacterial activity against bacteria is represented by the antibacterial ratio (R_a, %) and calculated using Eq. 5[35].

$$R_a = \frac{B-A}{B} \times 100\ \% \qquad \ldots (5)$$

where, A is the average number of bacteria on the graphite coatings, and B is the average number of bacteria on the control sample *i.e*., bare LCS.

The antibacterial activity of graphite-siloxane composite was studied by Total Viable Count (TVC) also called the plate count method. The bare LCS coupon, which was used as control, yielded 2.23×10^3 CFU/mL, which is very less compared to the samples G-400 ºC and G-600 ºC, which yielded 10 and 390 CFU/mL respectively, of the bacteria E.coli. In Fig. 6(d-f) the difference in the viable cell counts between the sample and control is visible. The graphite-siloxane composite cured at 400 ºC has almost no bacteria growth (Fig. 6(e)) even though 5µl of 10^8 E.coli. cells were inoculated on its surface and kept overnight for growth in the nutrient broth medium (Fig. 6(e)).

This shows the strong antibacterial action of the composite material. Even the G-600 ºC sample showed lesser growth compared to the bare LCS. Although the mechanism of action has not been established for this composite material, the past literature suggests that graphite has a powerful oxidative capacity towards glutathione (an antioxidant in bacteria) causing oxidative stress that kills the bacterial cells[19]. Also, several siloxane composites have proved to have antimicrobial properties due to their membrane disruption-causing ability[36-38]. It is also known that hydrophobic surfaces resist bacterial cell adhesion and hence with an increase in hydrophobicity, antibacterial efficiency will increase[39]. It may be one of the reasons why the G-400 ºC sample shows the highest hydrophobicity and antibacterial action. Bare LCS is hydrophilic and shows no or minor antibacterial activity. G-600 ºC is in between these two. The hydrophobic surface of G-600 ºC renders an antibacterial activity; however, the presence of micro-cracks on the surface makes it lesser efficient as compared to G-400 ºC.

Further, the attached bacteria on the bare LCS and G-400 ºC coated surface are investigated using FE-SEM. Fig. 7(a-b) displays the electron microscopic images of the samples examined using E.coli bacteria,

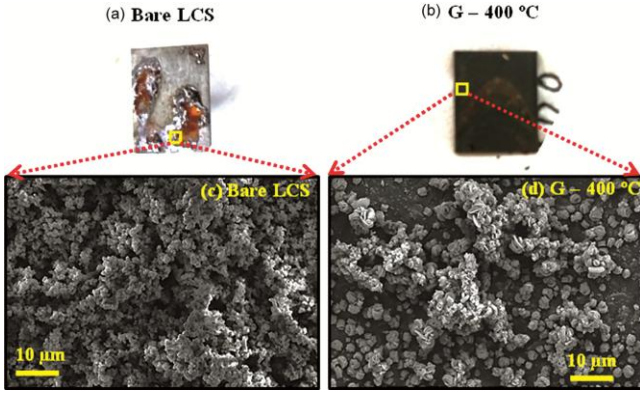

Fig. 7 — (a&b) show the digital images of the bare LCS and electrophoretically deposited graphite- siloxane composite coated surfaces, and (c-d) display the FE-SEM images of E.coli bacteria incubated on the low magnification of bare LCS and electrophoretically deposited graphite- siloxane composite coatings heat-treated at 400 ºC after antibacterial tests.

and Fig. 7(c-d) shows the corresponding FE-SEM images of their surface morphologies. The bare LCS has a dense bacteria growth (Fig. 7(c)), compared to the G-400 ºC coating (Fig. 7 (d)). Nevertheless, some dead bacteria are still observed on the surface of the bare LCS. However, the morphology of bacterial cells is distorted, indicating that the cells are under stress and mostly appear inactivated, in the case of a G - 400 ºC coated surface.

Figure 8 summarizes the correlation among hydrophobicity, corrosion resistance, and antibacterial properties of G-400 ºC coating. The corrosion mechanism of EPD graphite coating post-treated at 400 ºC is represented in Fig. 8(e). A stable composite coating forms a barrier for the diffusion of corrosive NaCl electrolytes, thus imparting corrosion resistance. In this study, G-400 ºC coating appears as the most stable, protective layer due to grain refinement and the hydrophobic nature of the surface. The combination of the presence of graphite and increased hydrophobicity onto the G-400 ºC coating surfaces resist bacterial cell adhesion as evidenced in Fig. 8(f) and leads to an increase in anti-bacterial properties.

To further understand the hydrophobic behaviour of G-400 ºC coating DFT based simulations are done. To obtain the LCS structure for simulation purpose initially we have selected the most stable α-Fe allotrope of iron. The basic unit cell is the BCC lattice with the space group p1 and the optimized lattice parameters a=b=c= 2.86 Å. After the relaxation of bulk unit cell, we have obtained the one of the intense XRD peak (110) as a plane suitable for further calculations. To mimic the LCS structure we have substituted around the four Fe atoms with carbon which comes around 3.125 at. % (4 atoms of carbon with 28 atoms of Fe). To avoid the complexity of simulations single layer graphene sheet is taken instead of graphite, which may not affect the results much. Now to study the hydrophobic nature, the water molecule is added to the LCS, LCS+Graphene and LCS+Graphene+Siloxane layers. These composites represent the coating of Graphene and siloxane over the low carbon steel. Initially, the water molecule was put at a distance of 2.5Å away above the plane of LCS and its composites. Once the optimization was done the water molecule get shifted as shown in Fig. 9(a-c).

It is seen that the distance of water molecule from LSC has goes on increasing with the addition of

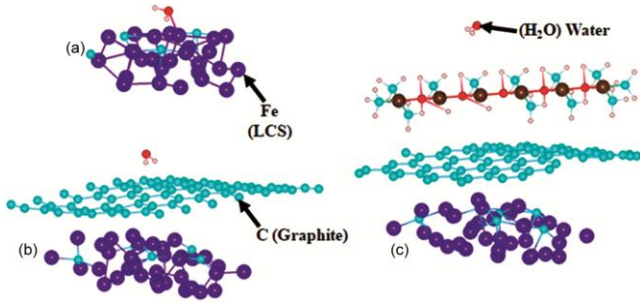

Fig. 9 — The geometrically optimized structures of (a)LCS+H_2O, (b) LCS+Graphene+H_2O and (c) LCS+Graphene+Siloxane+H_2O; Red, pink, cyan and violet represents O, H, C and Fe atoms respectively.

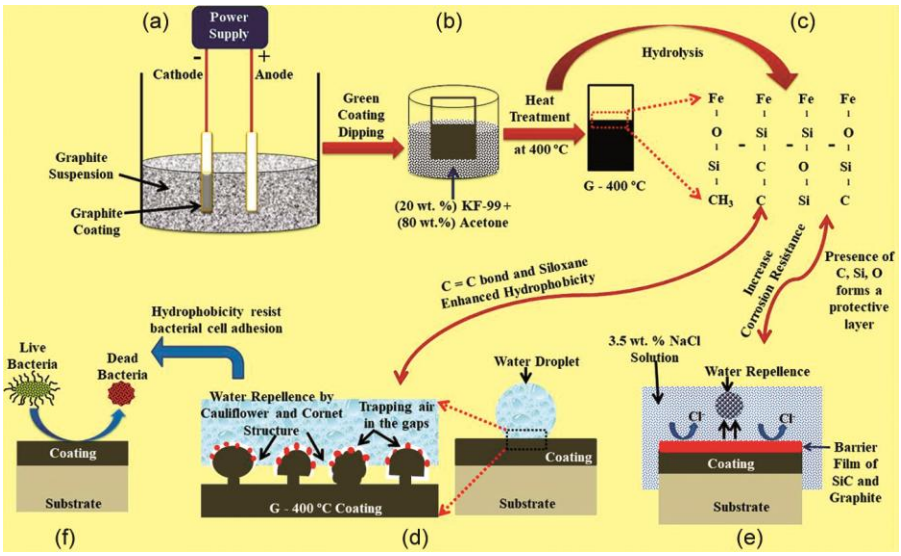

Fig. 8 — Schematic illustration of (a-c) Electrophoretic deposited graphite coatings process along with heat-treated at 400 ºC, (d) mechanism behind hydrophobicity, (e) Corrosion mechanism in 3.5 wt. % NaCl solution, and (f) anti-bacterial effect onto the G-400 ºC coating.

Composite layers to LCS and it is highest in case of LCS+Graphene+Siloxane. This is one of the clear indication that the interaction of water molecule has been reduced gradually with the addition of Graphene and Graphene/siloxane. To corroborate these findings, the adsorption energies of water molecule with all the composites are tabulated in Table 3, The -Ve sign in the adsorption energy indicates exothermic process whereas positive sign implies endothermic process. From Table 3, it may be concluded that the adsorption is most negative in case of bare LCS so the bonding and interaction is strongest and its hydrophilic in nature whereas the it is nearly zero and positive for other two composites implying that these composite are hydrophobic with higher weigthage for LCS+Graphene+Siloxane composite. The details of charge transfer are obtained using Bader charge partitioning[40] by considering the charge transfer between H_2O and LCS composites. The details of charge transfer are provided in Table 3. Here the charge gain by water molecule is highest in case of H_2O adsorbed on bare LSC while it is minimal in case of LSC+Graphene and zero in case of LCS+Graphene+Siloxane. So it signifies the strongest interactions with LSC (hydrophilic) with no interactions (hydrophobic) when both siloxane and graphite are attached with LSC.To visualize the spatial distribution of charge density, we have plotted the isosurface plots for these systems in Fig. 10. In these plots isovalue is fixed at 0.015e for all the composites. The yellow color represents the charge losing portion of the layers LSC, LCS+Graphene and LCS+Graphene+Siloxan in Fig. 10(a-c), respectively. It is noticed that the yellow portion indicating charge transfer reduces from LSC to LSC+graphene and almost vanishes for LCS+Graphene+Siloxan (Fig. 10(c)) signifying hydrophobic nature in LCS+ Graphene+Siloxan supporting the experimental data.

To get insights into the water molecule interaction at orbital level, the partial density of states (PDOS) plot for O 2*p* orbital of water in different configurations of LCS composites and also for isolated H_2O are plotted. From plots in Fig. 11, it may be said that the O 2p orbital of H_2O has shown the clear gain of states near fermi level for LCS+H_2O which again confirms the most active interactions and hydrophobic nature. Meanwhile the reduction of states has been observed in case of LCS+graphene which is the resultant of less interaction owing to the lower adsorption energy for H_2O. For the case of LCS+Graphene+Siloxan, The O 2p orbital of water molecule is similar to that of isolated water molecule signifying no interactions as now LCS+Graphene+ Siloxan composite become hydrophobic.

Table 3 — Adsorption energy and charge gain by water molecule on various structures.

System	H2O adsorption energy (eV)	Charge gain by H2O (e)
LCS	-9.98	0.02
LCS+Graphene	-0.007	0.005
LCS+Graphene+Siloxane	0.51	0.0

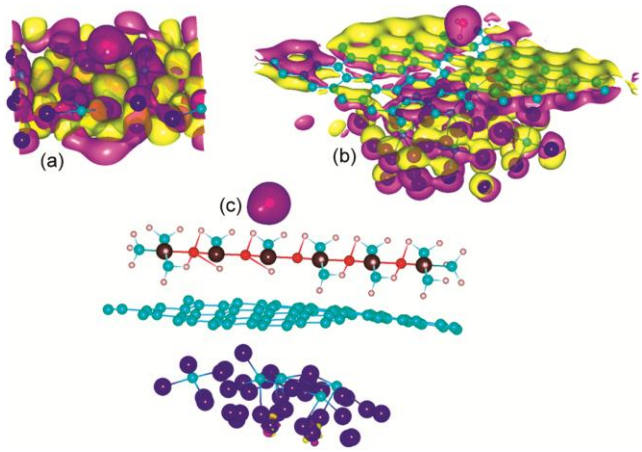

Fig. 10 — The isosurface plots for isovalue of 0.015e for (a) LCS+H_2O (b) LCS+Graphene+H_2O and (c) LCS+Graphene+ Siloxane+H_2O; yellow indicates charge loss region.

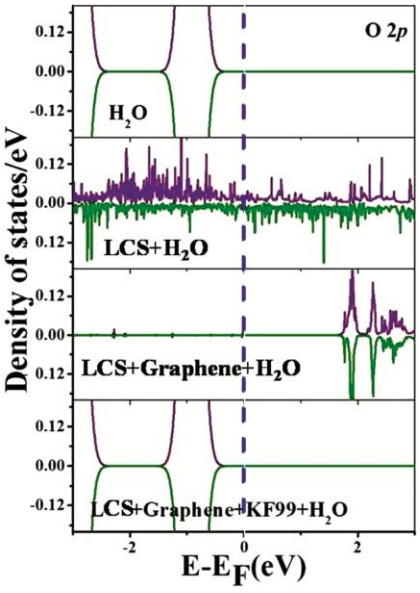

Fig. 11 — Partial density of states (PDOS) plots for O 2p orbital of isolated H_2O and its combination with LCS composites.

4 Conclusion

Electrophoretically deposited graphite-siloxane composite coatings are successfully fabricated. The FT-IR advocated the formation of Fe-O-Si and Fe-O-C bonds which confirms the bonding of the coating with the substrate. G-400 ºC coating showed an outstanding reduction in the corrosion rate by 79.32 % compared to the bare LCS in 3.5 wt. % NaCl solution. This improvement is accredited to the grain refinement, chemical inertness of graphite and formation of SiC, and the coatings hydrophobic nature. Further, G-400 ºC coating shows the best antibacterial property compared to bare LCS and G-600 ºC coating.

The hydrophobic nature of the coating material Graphite+Siloxane has been verified with the help of first principle calculations. The weakening of interaction between O 2*p* orbital of H_2O molecule with the addition of Graphite-Siloxane composite converts the LCS into a suitable hydrophobic material. Computed adsorption energy for water molecule, charge density iso-surface plot and partial density of states analysis for O 2p orbital reveal strong interactions of H_2O with LCS (hydrophilic), less interactions with LSC+graphene and no interactions with LCS+Graphene+Siloxan (hydrophobic) corroborating the experimental findings. The developed coating shows superior corrosion resistance and an antimicrobial activity that makes it a perfect candidate for studying its practical applications in the marine engineering sector, where very high corrosion resistance is needed. However, at the same time, it should be kept in mind that such coatings may not be suitable for tribological applications because of the lower thickness of the coating. One of the possible future tasks with this coating could be to increase the thickness of the coating without sacrificing the coating quality for tribological application. This work also opens up the possibility of further research on increasing the contact angle of the coating surface beyond 160^{o} to make the surface perfectly non-wetting in nature using suitable soft-chemical or physical methods.

Acknowledgment

Swarnima Singh and Bimal Prasad Singh acknowledge the Council of Scientific and Industrial Research (CSIR), New Delhi, for financial support (project number: ES-02). Sriparna Chatterjee acknowledges Council of Scientific and Industrial Research (CSIR), India, for financial support (13(9205-A)/2021-POOL). The authors also thank Dr. Laxmidhar Besra and N. Usha Kiran for their support and valuable feedback during the study.

Authors are grateful to the BARC supercomputing facility and their staff for the facility.

Reference

1 Qian M, Soutar A M, Tan X H, Zeng X T & Wijesinghe S L, *Thin Solid Films*, 517 (2009) 5237.
2 Niu L, Guo R, Tang C, Guoa H & Chen J, *Surf Coat Tech*, 300 (2016) 110.
3 He J, Sirois D, Li S, Sullivan M A, Wikle C & Chin B A, *J Mater Process Technol*, 232 (2016) 165.
4 Singh S, Pandey K K, Bose S K & Keshri A K, *Surf Coat Tech*, 396 (2020) 125964.
5 Yang W, Li Q, Xiao Q & Liang J, *Prog Org Coat*, 89 (2015) 260.
6 Pali L S, Ganesan P & Garg A, *Sol Energy*, 133 (2016) 339.
7 Wang L, Gao Y, Xu T & Xue Q, *Appl Surf Sci*, 252 (2006) 7361.
8 Chanda U K, Behera A, Roy S & Pati S, *Int J Hydrogen Energ*, 43 (2018) 23430.
9 Aghdam A S, Allahkaram S R & Mahdavi S, *Surf Coat Tech*, 281 (2015) 144.
10 Park J H & Park J M, *Surf Coat Tech*, 254 (2014) 167.
11 Shornikova O N, Kogan E V, Sorokina N E & Avdeev V V, *Russ J Phys Chem A*, 83 (2009) 1022.
12 Mokhena T C, Mochane M J, Sefadi J S, Motloung S V & Andala D M, Thermal Conductivity of Graphite-Based Polymer Composites, *Impact of Thermal Conductivity on Energy Technologies*, (2018).
13 Arun S, Hariprasad S, Saikiran A, Ravisankar B, Parfenov E V, Mukaeva V R & Rameshbabu N, *Surf Coat Tech*, 363 (2019) 301.
14 Zhang J, Piao Z Y, Liu S Y, Su S W & Deng L J, *Eng Fail Anal*, 97 (2019) 408.
15 Zhang X, Epifanio M & Marsili E, *Electrochim Acta*, 102 (2013) 252.
16 Singh B P, Nayak S, Nanda K K, Jena B K, Bhattacharjee S & Besra L, *Carbon*, 61 (2013) 47.
17 Singh Bimal P, Jena B K, Bhattacharjee S & Besra L, *Surf Coat Tech*, 232 (2013) 475.
18 Dey S, Chatterjee S, Singh B P, Bhattacharjee S, Rout T K, Sengupta D K & Besra L, *Surf Coat Tech*, 341 (2018) 24.
19 Liu S, Zeng T H, Hofmann M, Burcombe E, Wei J, Jiang R, Kong J & Chen Y, *ACS Nano*, 5 (2011) 6971.
20 Singh S, Sribalaji M, Isekar N P, Joshi S, Sundararajan G, Singh R & Keshri A K, *Appl Surf Sci*, 364 (2016) 264.
21 Kiran N U, Dey S, Singh B P & Besra L, *Coatings*, 7 (2017) 214.
22 Kresse G & Hafner J, *Phys Rev B*, 47 (1993) 558(R).
23 Kresse G & Hafner J, *Phys Rev B*, 49 (1994) 14251.
24 Kresse G & Furthmüller J, *Phys Rev B*, 54 (1996) 11169.
25 Kresse G & Furthmüller J, *Set Comput Mater Sci*, 6 (1996) 15.
26 Perdew J P, Burke K & Ernzerhof M, *Phys Rev Lett*, 77 (1996) 3865.
27 Monkhorst H J & Pack J D, *Phys Rev B*, 13 (1976) 5188.
28 Kwon H, Lee G G, Kim S G, Lee B W, Seo W C & Leparoux M, *Mat Sci Eng A*, 632 (2015) 72.

29 Tail F C, Lee S C, Wei C H & Tyan S L, *Mater Trans*, 47 (2006) 1847 .
30 Sahnesarayi M K, Sarpoolaky H & Rastegari S, *Surf Coat Tech*, 258 (2014) 861.
31 Lee Y J & Joo H J, *Surf Coat Tech*, 180 –181 (2004) 286.
32 Rabizadeh T, Allahkaram S R & Zarebidaki A, *Mater Des*, 31 (2010) 3174.
33 Tsui Y C, Doyle C & Clyne T W, *Biomaterials*, 19 (1998) 2031.
34 Nishimotoab S & Bhushan B, *RSC Adv*, 3 (2013) 671.
35 Yin L, Fu Z, Li Y, Liu B, Lin Z, Lu J, Chen X, Han X, Deng Y, Hu W, Zou D & Zhong C, RSC Adv, 9 (2019) 4521.
36 Zhou N, Xu D, Zhang J, Ma Y, Yuan J & Shen J, *J Biomed Mater Res A*, 100 (2012) 1623.
37 Jon´ca1J, Tukaj C, Werel1W, Mizerska U, Fortuniak W & Chojnowski J, *J Mater Sci Mater Med*, 27 (2016) 55.
38 Bao Y, Guo J, Ma J, Li M & Li X, *J Mol Liq*, 242 (2017) 8.
39 Zhang X, Wang L & Levänen E, *RSC Adv*, 3 (2013) 12003.
40 Tang W, Sanville E & Henkelman G, *J Phys: Condens Matter*, 21 (2009) 084204.